JCTC Journal of Chemical Theory and Computation

Article

Cite This: J. Chem. Theory Comput. XXXX, XXX, XXX−XXX

pubs.acs.org/JCTC

Transferable, Polarizable Force Field for Ionic Liquids

Kateryna Goloviznina,[†] José N. Canongia Lopes,[‡] Margarida Costa Gomes,[†] and Agílio A. H. Pádua*[,†]

[†]Laboratoire de Chimie, École Normale Supérieure de Lyon & CNRS, 69364 Lyon, France

[‡]Centro de Química Estrutural, Instituto Superior Técnico, Universidade de Lisboa, 1049-001 Lisboa, Portugal

ABSTRACT: A general, transferable, polarizable force field for molecular simulation of ionic liquids (ILs) and their mixtures with molecular compounds is developed. This polarizable model is derived from the widely used CL&P fixed-charge force field that describes most families of ILs, in a form compatible with OPLS-AA, one of the major force fields for organic compounds. Models for ILs with fixed, integer-ionic charges lead to pathologically slow dynamics, a problem that is corrected when polarization effects are included explicitly. In the model proposed here, Drude-induced dipoles are used with parameters determined from atomic polarizabilities. The CL&P force field is modified upon inclusion of the Drude dipoles to avoid double-counting of polarization effects. This modification is based on first-principles calculations of the dispersion and induction contributions to the van der Waals interactions using symmetry-adapted perturbation theory (SAPT) for a set of dimers composed of positive, negative, and neutral fragments representative of a wide variety of ILs. The fragment approach provides transferability, allowing the representation of a multitude of cation and anion families, including different functional groups, without the need to reparametrize. Because SAPT calculations are expensive, an alternative predictive scheme was devised, requiring only molecular properties with a clear physical meaning, namely, dipole moments and atomic polarizabilities. The new polarizable force field, CL&Pol, describes a broad set of ILs and their mixtures with molecular compounds and is validated by comparisons with experimental data on density, ion diffusion coefficients, and viscosity. The approaches proposed here can also be applied to the conversion of other fixed-charge force fields into polarizable versions.

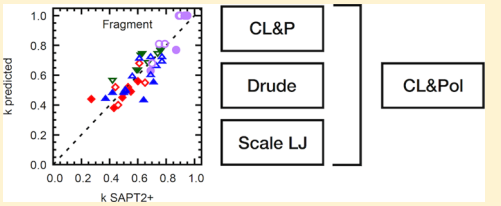

Downloaded via UNIVERSIDADE DE LISBOA 00700 on October 4, 2019 at 11:57:41 (UTC).
See https://pubs.acs.org/sharingguidelines for options on how to legitimately share published articles.

1. INTRODUCTION

Molecular simulation has been essential in the study of the physical chemistry of ionic liquids (ILs). This class of materials became available in the past 2 decades with potential for breakthroughs in various domains and a number of industrial-scale processes already in place that brought major gains in efficiency and sustainability.[1,2] IL materials include mixtures rich in ions, such as deep eutectic solvents (DES), which are obtained by combining an organic salt with a molecular compound. ILs and DES are complex liquids formed by large organic ions with delocalized electrostatic charge, conformational flexibility, and asymmetric molecular shapes, which also contain aromatic groups, hydrogen bonds, apolar side chains, or combinations thereof. The ordering and dynamics of the liquid phases, and the ensuing properties, are the result of a subtle balance between Coulomb and van der Waals interactions. Because of this variety and complexity, modeling ILs at the molecular level are challenging. Also, the time and length scales needed to represent the medium-range ordering (10^1 to 10^2 nm), and the diffusion and reordering of solvation or interfacial layers (10^1 to 10^2 ns) are unattainable in practice using quantum electronic structure methods, especially when dealing with noncovalent interactions that require highly accurate energies. Thus, molecular simulation using atomistic force fields is the computational method of choice to study IL systems because it presents a reasonable compromise between computational cost and level of detail in the molecular structures and interactions.

Atomistic force fields have been developed that are general and transferable, therefore able to simulate many families of ions.[3−5] These have mathematical forms compatible with well-known force fields for organic compounds (OPLS-AA[6] and AMBER/GAFF[7]), enabling the study of systems containing many other compounds. This is important in order to provide understanding about physical and chemical properties and to devise structure−property relations for IL materials. In the first generation of force fields,[5] the Coulomb terms are modeled by fixed partial charges on the atomic sites. This is probably their main limitation because although structural and solvation properties are rather well predicted, the dynamics is generally too sluggish, leading to calculated diffusion coefficients that are largely below the experimental values, and viscosities that are too high.[8] Modifying these force fields by scaled-down ionic charges,[9−11] for example, down to ±0.8 e, is a practical and widely used fix to improve the calculation of transport properties without adding computational overhead. However, charge-scaling has adverse effects on structural and dielectric quantities,[12,13] often leading to liquid densities that are lowered by around 5% and to less intense structural peaks of the nearest-neighbor layers (as we will show below), while not improving the dielectric response and the screening behavior from that of fixed-charge models.[13]

Received: July 10, 2019
Published: September 17, 2019

© XXXX American Chemical Society

DOI: 10.1021/acs.jctc.9b00689
J. Chem. Theory Comput. XXXX, XXX, XXX−XXX

Including polarization (induction) explicitly is a significant step toward improving molecular force fields in general[14−18] and for ILs in particular.[19−21] This field has just been the topic of a detailed review article.[22] Polarization can be represented explicitly using a number of methods, mainly fluctuating charges, induced point dipoles, or Drude-induced dipoles.[22] (Drude dipoles are formed by two point charges of opposite sign connected by a spring, giving rise to an induced dipole when subject to an electrostatic field.) The last two methods are equivalent and offer some advantages with respect to fluctuating charges: they allow for out-of-plane induction in planar molecules and can easily mix polarizable and nonpolarizable atoms; fluctuating charges, however, require no additional particles and should be computationally faster. In this work, we chose to include polarization explicitly using Drude-induced dipoles because this approach has been the one most often used by the community studying ILs and is implemented in a number of molecular dynamics (MD) codes, such as NAMD,[23] LAMMPS,[24] GROMACS,[25] and OpenMM.[26] Essentially, atomic polarizabilities are all the additional information required to set up a polarizable simulation, which are parameters with a clear physical sense, available for ILs.[27,28]

Although the methods for polarizable simulations of ILs exist, parameterizing from scratch, a transferable, polarizable force field is a huge task. Alternatively, adding polarization terms to a fixed-charge force field implies the modification of the nonbonded attractive energies [represented by Lennard-Jones (LJ) or equivalent potentials describing van der Waals interactions][8] in order to remove a double counting of the induction effects, which are included implicitly in the empirical LJ potential. In a polarizable model, the LJ potential should account only for London dispersion, the polarization being represented explicitly by the induced dipoles. By evaluating the individual dispersion and induction components, LJ terms could be scaled in existing general force fields before including polarization explicitly in a consistent manner. This strategy was attempted in our previous study,[8] based on symmetry-adapted perturbation theory (SAPT)[29,30] to resolve the induction and dispersion contributions. The aims of this work are to extend this strategy and to devise a scheme of general applicability to transform the existing fixed-charge force fields into polarizable versions without the need for expensive first-principles calculations, thus enabling the simulation of ILs with much better prediction of both equilibrium and transport properties.

2. FRAGMENT APPROACH

We report here a set of SAPT calculations to resolve the different contributions to interaction energies on 46 dimers composed of ions, representative of different families of ILs, and also of neutral molecules. Our aim is to generate a sufficiently large data set to develop a predictive scheme. By parameterizing fragments separately and not entire ions,[5] we can achieve the necessary transferability to describe broad families of ions without the need for a specific parameterization effort for each individual compound. The structural formulae of the ion families considered here are given in Figure 1.

The fragment approach followed[8] allows to treat a smaller set of building blocks. For example, most cations in ILs are formed by a charged head group and one or several side chains with various possible lengths. Therefore, 1-ethyl-3-methylimidazolium ($C_2C_1im^+$), 1-ethylpyridinium (C_2Py^+), 1,1-dimethylpyrrolidinium ($C_1C_1pyr^+$), and tetramethylammonium (N_{1111}^+) cations were considered as representative head groups for

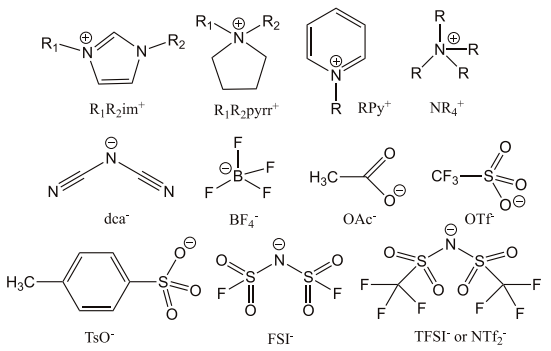

Figure 1. Structural formulae of cations and anions of ILs.

imidazolium, pyridinium, pyrrolidinium, and quaternary ammonium ILs, respectively. Butane (C_4H_{10}) was used as the representative fragment for alkyl side chains, and from its atom types, chains of different lengths can be created. From our previous work in force field development for ILs,[5] we learnt that the influence of a charged group along an alkyl side chain extends up to two bonds along the chain, so the C_2 and H_1 atoms connected to the C_1 require specific parameters, especially partial charges. Further along an alkyl side chain, the parameters can be taken considered as equal to those of *n*-alkanes.

Concerning anions, tetrafluoroborate, dicyanamide (dca^-), and bis(trifluoromethanesulfonyl)amide (Ntf_2^-), bis(fluorosulfonyl)imide (FSI^-), trifluoromethanesulfonate or triflate (OTf^-), and acetate (OAc^-) were treated as entire ions. General alkylsulfonates can in turn be built by combining the parameters of the sulfonate head group with those of an alkyl side chain.[31] Here, *p*-toluenesulfonate or tosylate (TsO^-) was split into toluene (Tol) and methanesulfonate or mesylate (MsO^-) fragments.

The fragment set considered also includes neutral polar molecules, such as acetonitrile (AN) and dimethyl sulfoxide (DMSO), slightly polar dimethoxyethane (DME), which is a monomer unit of polyethylene oxide, nonpolar hexane (C_6H_{14}), and aromatic benzene (Bz).

We performed SAPT calculations of the potential energy of interaction, for dimers composed of selected fragments of ionic or molecular species, from which we obtained a sufficiently large set of values for dispersion and induction energies. Then, we proceeded to generate MD trajectories of ILs and their mixtures with molecular compounds to calculate condensed-phase equilibrium and transport properties. These are compared to experimental values, in order to assess the soundness of our strategy through the predictive ability of the polarizable force field.

3. COMPUTATIONAL METHODS AND FORCE FIELD

Geometries of isolated molecules, ions, and subsequently dimers were optimized using dispersion-corrected density functional theory[32] at the B97-D3/cc-pVDZ level. The potential energy curves for each dimer were calculated using sSAPT0/jaDZ[33] at a series of the distances between the monomers, while keeping their geometries fixed. At the distance corresponding to the potential energy minimum, energies were calculated at the SAPT2+/aDZ[33] level to obtain more accurate values for the dispersion and induction energies. SAPT calculations were performed using Psi4.[34] Atomic partial charges and dipole moments of molecules and fragments were obtained, on optimized geometries with Gaussian,[35] using the CHelpG[36]

DOI: 10.1021/acs.jctc.9b00689
J. Chem. Theory Comput. XXXX, XXX, XXX−XXX

method with MP2/cc-pVTZ(-f) densities. The dipole moment of charged fragments was calculated using coordinates with origin on the center of mass (the "standard orientation" of Gaussian).

MD simulations of cubic boxes containing 300 ion pairs for pure ILs or $300(1-x)$ ion pairs and $300x$ solvent molecules for mixtures with x solvent mole fraction were performed with LAMMPS.[37] Initial configurations were generated using the fftool[38] and packmol[39] utilities. A cutoff of 12 Å was considered for the LJ potential, with tail corrections for energy and pressure. The particle−particle particle−mesh method was used to evaluate electrostatic energies with the accuracy of 1×10^{-5}. Bonds terminating in hydrogen atoms were constrained using the SHAKE algorithm. The time step was of 1 fs. The systems were equilibrated for 2 ns in the NpT ensemble, following which 10 ns production runs were performed in the NpT and NVT ensembles using Nosé−Hoover thermostat and barostat. Different temperatures were chosen for different systems according to the availability of experimental data for comparison and to the viscosity of the liquid, in the range 298−353 K. Pressure was kept at 1 bar in all runs.

The fixed-charge force field that serves as the basis for the present development is the CL&P force field,[3,5,40,41] with revised LJ parameters for fluorinated sulfonylimide anions[42] that yield more accurate liquid densities with respect to our previous paper,[8] in particular for Ntf_2^--based ILs. Molecular compounds were represented by the OPLS-AA force field.[6]

Adding explicit polarization requires knowledge of atomic polarizabilities, which we took from the recent work of Schröder.[28] All heavy atoms were considered as polarizable, while polarizability of hydrogen atoms was merged onto the polarizability of the atoms to which they are bonded. The mass of Drude particles (DPs) was set at $m_D = 0.4$ au and the force constant of the harmonic spring between Drude cores (DC, the polarizable atom sites) and DP set at $k_D = 4184$ kJ·mol^{-1}. The partial charges of the DPs were calculated from the polarizabilities according to $\alpha = q_D^2/k_D$.[14] The total charge of the DC plus the DP is equal to the initial charge of the (nonpolarizable) atom. Thole damping functions[24,43] were employed to reduce at short range the electrostatic interactions between induced dipoles, in order to avoid excessive correlation between neighboring DP. An universal value of the parameter $a = 2.6$ was chosen according to the functional form given in the literature.[24,44] The relative motion of DP with respect to their DC was regulated at an equivalent temperature of 1 K using a specific thermostat.[14,24] This is an extended Lagrangian method that allows the DP to follow closely the trajectory of a relaxed system. The input files for LAMMPS with the polarizable force field were prepared using the polarizer tool,[24,38] which converts nonpolarizable input files to the polarizable ones. Simulations with Drude-induced dipoles can be enabled in LAMMPS by activating the USER-DRUDE package.[24]

Dynamic properties, namely, diffusion coefficients and viscosities, were evaluated from equilibrium trajectories using the Einstein and Green−Kubo relations, following the recommendations of a recent review.[45] Diffusion coefficients were calculated from mean-squared displacements using Einstein's relation

$$D = \lim_{x\to\infty} \frac{1}{6}\frac{\mathrm{d}}{\mathrm{d}t}\langle(\mathbf{r}(t) - \mathbf{r}(0))^2\rangle \tag{1}$$

which yielded converged values within the duration of the trajectories. However, the evaluation of shear viscosity using the Green−Kubo relation

$$\eta = \frac{V}{kT}\int_0^\infty \langle p_{xy}(t)p_{xy}(0)\rangle \mathrm{d}t \tag{2}$$

was more difficult to converge because the autocorrelation function (ACF) in the integrand becomes noisy at long times and the viscosity values from integrating the three off-diagonal components, p_{xy}, p_{yz}, and p_{zx}, become inconsistent. We smooth the tail of the ACF with an exponential decay function

$$S_{\mathrm{ACF}}^{\mathrm{f}}(t) = a\,\exp(-t^{\beta}) \tag{3}$$

where a and β are determined from fit to the nonoscillatory decay section of the ACF. This is among the functional forms suggested,[45] which it led to good fits of our ACF data. Integration was performed using the raw values of pressure components up to a switching time, after which the noisy tail of the ACF was replaced by the fitting function. This switching time was around $t_s = 1$ ps. This procedure yielded satisfactory results, and the viscosities we report are the average between the integrations of the three off-diagonal components, with the associated standard deviation. We found that fitting the long tail of the ACF led to more consistent results than fitting the tail of the running integral.[45]

4. EVALUATION OF INDUCTION AND DISPERSION

The SAPT calculations of the repulsive, electrostatic, induction, and dispersion terms of the potential energy of interaction were performed for 46 dimers composed of charged and neutral fragments: 13 cation−anion fragment dimers, 9 cation−neutral dimers, 14 anion−neutral dimers, and 10 neutral−neutral dimers. Two examples, a cation−anion pair $C_2C_1im^+\cdots BF_4^-$ and a neutral molecule-ion $C_4H_{10}\cdots BF_4^-$, are illustrated in Figure 2 with the energy values reported in Table 1. The full set of SAPT calculations is provided in the Appendix.

We evaluated a k_{ij} factor, which is the ratio between the dispersion contribution and the sum of dispersion and induction

$$k_{ij} = \frac{E_{\mathrm{disp}}}{E_{\mathrm{disp}} + E_{\mathrm{ind}}} \tag{4}$$

This is the factor by which the LJ attractive energy in the nonpolarizable force field must be scaled, in order to retain only dispersive terms and exclude polarization contributions from the LJ potential, as induction will be explicitly represented by the Drude-induced dipoles. Therefore, in the polarizable force field, the LJ ϵ parameters will be scaled by a factor k_{ij}. The scaling factors are evaluated per fragment; therefore, for the ions and molecules that will be considered in applications, different scaling factors may be applied between atom groups within the ions or molecules. We considered only dimers that can be found at distances characteristic of first solvation or coordination shells, that is, cation−anion, ion−neutral, and neutral−neutral, so we did not perform calculations between same-charge fragments whose interactions are dominated by the repulsive electrostatic terms and are usually found at large separations.

The scaling factors from SAPT are derived from gas-phase dimers, so we sought to evaluate the relative dispersion and induction contributions in condensed-phase simulations of ILs and their mixtures with molecular compounds. We performed MD simulations of 11 ILs based on $C_2C_1im^+$, $C_4C_1im^+$, $C_6C_1im^+$, and $C_4C_1pyrr^+$ cations and BF_4^-, dca^-, and Ntf_2^-

DOI: 10.1021/acs.jctc.9b00689
J. Chem. Theory Comput. XXXX, XXX, XXX−XXX

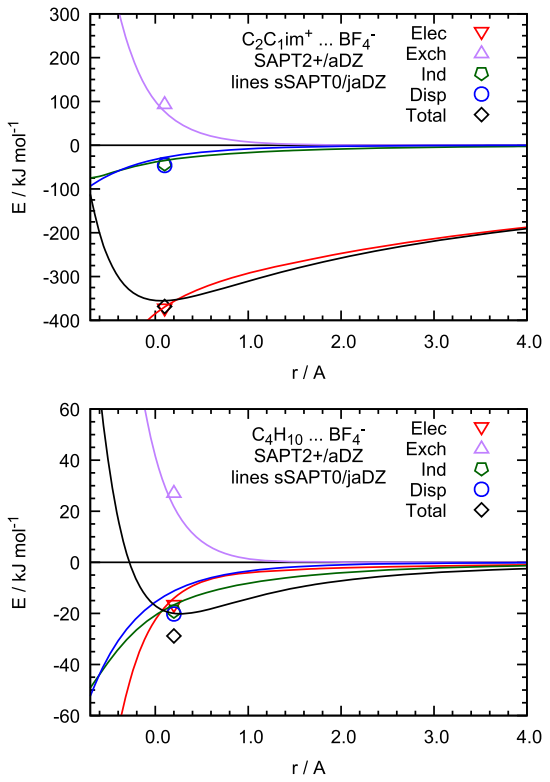

Figure 2. Energy decomposition of the interaction potential of BF_4^- with $C_2C_1im^+$ and with C_4H_{10} obtained from SAPT calculations. Lines correspond to calculations at the sSAPT0/jaDZ level and symbols to more accurate calculations at the equilibrium distance at the SAPT2+/aDZ level.

Table 1. Dispersion and Induction Energies of Dimers Obtained with Different SAPT Levels at the Distance Corresponding to the Potential Energy Minimum[a]

method	E_{tot}	E_{disp}	E_{ind}	k_{ij}
C_4H_{10}···BF_4^-				
sSAPT0/jaDZ	−20.0	−11.2	−19.1	0.40
SAPT2+/aDZ	−28.8	−20.2	16.6	0.51
$C_2C_1im^+$···BF_4^-				
sSAPT0/jaDZ	−355.3	−28.1	−34.9	0.45
SAPT2+/aDZ	−368.4	−46.3	−42.6	0.52

[a]The factor k_{ij} corresponds to the fraction of dispersion in non-Coulomb attraction. Energies are given in kJ·mol^{-1}.

anions. The present data sets on SAPT calculations on dimers and MD simulations on liquid systems considerably expand our previous report[8] on eight dimers and three ILs.

The following nomenclature was used to identify the different force field settings: (a) FixQ: the original fixed-charge CL&P force field; (b) Drude: CL&P force field with DP added but no LJ scaling; (c) SDrude: CL&P force field with DP added and scaled ϵ_{ij} by the k_{ij} factors. The cohesive energy (with respect to isolated ions), LJ, and electrostatic energies (including long-range part) are presented in Table 2 and were evaluated through the expressions

$$\langle E_c \rangle = \langle E_{tot}^{IL} \rangle / N - \langle E_{tot}^{+} \rangle - \langle E_{tot}^{-} \rangle$$
$$\langle E_{LJ} \rangle = \langle E_{LJ}^{IL} \rangle / N - \langle E_{LJ}^{+} \rangle - \langle E_{LJ}^{-} \rangle$$
$$\langle E_{elst} \rangle = \langle E_{elst}^{IL} \rangle / N - \langle E_{elst}^{+} \rangle - \langle E_{elst}^{-} \rangle \quad (5)$$

where $\langle E^{IL} \rangle$ is the system total van der Waals or electrostatic energy averaged over the MD trajectory; $\langle E^+ \rangle$ and $\langle E^- \rangle$ correspond to the total van der Waals or electrostatic energy of a single cation or anion obtained from additional 10 ns *NVT* runs at the same temperature in a simulation box with 30 Å side. The induction contribution in the liquid-state systems can be evaluated as the change in electrostatic energy because of introducing DP, taking into account the self-energy of the Drude oscillators (which is the potential energy stored in the DC−DP harmonic bonds)

$$\langle E_{ind} \rangle \approx \langle E_{elst} \rangle - \langle E_{elst}(\text{FixQ}) \rangle - \langle E_{self} \rangle \quad (6)$$

The fraction of dispersion energy in nonbonded interactions in condensed phase can be evaluated through $K = \langle E_{LJ} \rangle / (\langle E_{LJ} \rangle + \langle E_{ind} \rangle)$, which can be compared with the effective scaling factors from SAPT, averaged per atom according to the fragments involved, $\langle k_{ij} \rangle$, presented in Table 2.

In general, the *K* values from the liquid-state simulations were found to be close to $\langle k_{ij} \rangle$, with differences below 0.1, which means that the SAPT calculations on isolated dimers are good predictors of the energy decomposition in condensed phases. An exception is found for [RC_1im][dca] ILs, for which the induction contribution in the liquid phase appears significantly larger than in the gas-phase dimers. We investigated the source of this discrepancy and found that in the optimized dimer geometry, the dicyanamide anion is placed above the imidazolium ring, in order to minimize the electrostatic energy of the pair, as shown in Figure 3. The most likely configurations in the liquid phase, however, are quite different, with the anions sitting close to the plane of the imidazolium ring (Figure 4) with hydrogen bonds being formed between the H atoms of the ring and the terminal N atoms of dicyanamide (Figure 5). Thus, we interpret the discrepancy in the values of the k_{ij} scaling factors as a result of the geometry of the isolated dimer, which is not representative of those in the liquid phase. Because our aim is to develop a general methodology, we opted to not fine-tune this step of geometry optimization of the dimers and instead assess the validity of this choice by the ability of the new model to predict equilibrium and transport properties of IL systems.

Using the k_{ij} scaling factors from SAPT calculations on fragment dimers thus provides a means to adapt an existing force field into a polarizable one, as shown in a previous feasibility report.[8] Predictions of equilibrium and transport properties of ILs and mixtures with molecular compounds will be presented below. Evaluation of scaling factors using SAPT2+ is nevertheless computationally demanding. For example, a single-point calculation of C_2Py^+···Ntf_2^- dimer at SAPT2+/aDZ level requires 75 GB of memory and takes 4.5 days on 16 processors.

5. PREDICTING DISPERSION SCALING FACTORS

The cost of SAPT calculations led us to propose a general predictive scheme to obtain the k_{ij} scaling factors from simple, readily calculated atom or fragment properties. The scaling factor can be expressed through the ratio between the induction and dispersion energies

$$k_{ij} = \left(1 + \frac{E_{ind}}{E_{disp}}\right)^{-1} \quad (7)$$

and these two terms can be evaluated from induction (Debye) and dispersion (London) forces.

DOI: 10.1021/acs.jctc.9b00689
J. Chem. Theory Comput. XXXX, XXX, XXX−XXX

Table 2. Cohesive Energy with Respect to Isolated Ions and LJ and Electrostatic Contributions from MD Trajectories Using Different Force Field Settings[a]

	$\langle E_c \rangle$	$\langle E_{LJ} \rangle$	$\langle E_{elst} \rangle$	$\langle E_{self} \rangle$	$\langle E_{ind} \rangle$	$\langle k_{ij} \rangle$	K
[C_4C_1im][BF_4] 343 K							
FixQ	−482.7	−62.2	−434.4	0.0	0.0	1.0	1.0
Drude	−422.8	−58.6	−433.9	17.3	−16.8	1.0	0.78
SDrude	−405.1	−34.5	−444.3	19.8	−29.7	0.52	0.54
[C_2C_1im][dca] 303 K							
FixQ	−492.1	−72.0	−429.7	0.0	0.0	1.0	1.0
Drude	−498.5	−68.3	−461.9	34.5	−66.7	1.0	0.51
SDrude	−484.1	−46.9	−473.6	36.9	−80.9	0.61	0.37
[C_4C_1im][Ntf_2] 323 K							
FixQ	−479.5	−117.6	−370.1	0.0	0.0	1.0	1.0
Drude	−419.1	−114.6	−361.3	36.4	−27.6	1.0	0.81
SDrude	−385.4	−79.4	−364.9	38.4	−33.3	0.70	0.70
[C_4C_1pyr][Ntf_2]343 K							
FixQ	−475.0	−114.6	−368.6	0.0	0.0	1.0	1.0
Drude	−412.8	−108.5	−350.9	34.8	−17.1	1.0	0.86
SDrude	−363.0	−64.9	−353.5	36.7	−21.7	0.64	0.75
[C_4C_1im][dca] 323 K							
FixQ	−493.5	−79.9	−422.5	0.0	0.0	1.0	1.0
Drude	−436.3	−74.7	−439.8	37.0	−54.3	1.0	0.58
SDrude	−416.8	−48.1	−453.6	43.6	−74.6	0.64	0.39
[C_4C_1pyr][dca] 323 K							
FixQ	−493.4	−79.8	−419.5	0.0	0.0	1.0	1.0
Drude	−428.6	−72.9	−419.5	29.8	−29.8	1.0	0.71
SDrude	−414.0	−43.9	−428.7	34.1	−43.3	0.60	0.50
[C_6C_1im][dca] 323 K							
FixQ	−502.1	−89.9	−419.5	0.0	0.0	1.0	1.0
Drude	−438.2	−84.1	−429.8	40.2	−50.5	1.0	0.62
SDrude	−419.3	−55.0	−446.5	47.8	−74.8	0.65	0.42
[C_2C_1im][Ntf_2] 323 K							
FixQ	−474.2	−108.4	−373.5	0.0	0.0	1.0	1.0
Drude	−473.1	−106.3	−384.7	34.5	−45.7	1.0	0.70
SDrude	−442.6	−74.2	−388.0	36.4	−51.0	0.65	0.59
[C_6C_1im][Ntf_2] 343 K							
FixQ	−482.3	−124.2	−367.1	0.0	0.0	1.0	1.0
Drude	−410.0	−120.6	−348.6	38.1	−19.6	1.0	0.86
SDrude	−377.1	−83.5	−352.3	40.2	−25.5	0.71	0.77
[C_2C_1im][BF_4] 323 K							
FixQ	−483.8	−54.8	−442.3	0.0	0.0	1.0	1.0
Drude	−486.4	−52.6	−458.7	13.8	−30.1	1.0	0.64
SDrude	−476.3	−34.5	−468.1	15.2	−41.0	0.52	0.46
[C_6C_1im][BF_4] 353 K							
FixQ	−485.2	−70.5	−431.1	0.0	0.0	1.0	1.0
Drude	−445.2	−69.8	−424.1	19.6	−12.5	1.0	0.85
SDrude	−428.9	−44.0	−437.4	22.5	−28.8	0.51	0.60

[a]FixQ: fixed-charge CL&P force field; Drude: polarization added to CL&P, no scaling; SDrude: Drude model with scaled ϵ_{ij} LJ parameter by k_{ij} from SAPT2+/aDZ. Energies given in kJ·mol^{-1}.

The induction energy between the two molecular or ionic fragments i and j, averaged over orientations, is given by[46]

$$E_{ind} = -\frac{Q_i^2\alpha_j + Q_j^2\alpha_i}{2r_{ij}^4} - \frac{\mu_i^2\alpha_j + \mu_j^2\alpha_i}{r_{ij}^6} - \dots \quad (8)$$

where α are the polarizabilities of the fragments, Q their net charges, and μ the dipole moments (we calculated the dipole moment of charged fragments using coordinates with origin on the center of mass). The distance r_{ij} is measured between the fragments. The first term in eq 8 is expected to dominate for charged fragments and the second for neutral but polar fragments.

The dominant dispersion energy between two monomers is

$$E_{disp} = -\frac{3}{2}\frac{I_iI_j}{I_i + I_j}\frac{\alpha_i\alpha_j}{r_{ij}^6} + \dots \quad (9)$$

and it depends on polarizabilities α and ionization energies I. The ratio between the induction and the dispersion energies thus takes the form

DOI: 10.1021/acs.jctc.9b00689
J. Chem. Theory Comput. XXXX, XXX, XXX−XXX

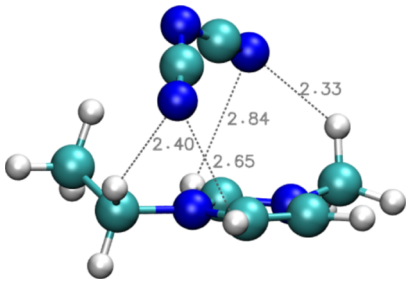

Figure 3. Optimized geometry of the isolated $C_2C_1im^+\cdots dca^-$ dimer showing that the anion is positioned above the plane of the imidazolium ring with no close interactions with the H atoms of the ring. The closest C−H···N approach observed with H_1 atoms is the alkyl side groups.

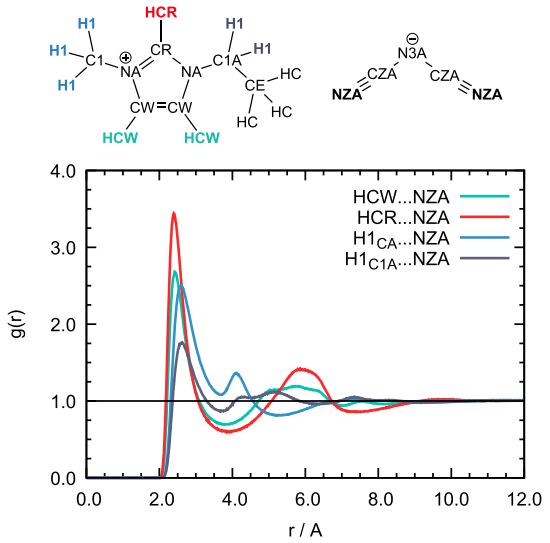

Figure 4. Radial distribution functions between hydrogen atoms of the cation and terminal nitrogen atoms of the anion of $[C_2C_1im][dca]$, showing closer distances and more intense peaks involving the H_{CR} and H_{CW} atoms, mainly the former. Results obtained from a 10 ns MD trajectory with the SDrude force field.

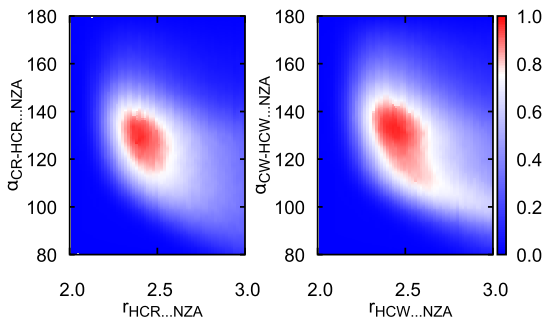

Figure 5. Probability contours revealing hydrogen bonds between the cation and anion in liquid $[C_2C_1im][dca]$, obtained from a 10 ns MD trajectory with the SDrude force field. The *x*-axes represent the distances between H atoms of the imidazolium rings and terminal N atoms from the dca^- anions. The *y*-axes represent the angles formed by the C−H···N hydrogen bonds. The most likely angles are around 130−135°.

$$\frac{E_{ind}}{E_{disp}} = c_0 r_{ij}^{\ 2} \frac{Q_i^{\ 2}\alpha_j + Q_j^{\ 2}\alpha_i}{\alpha_i\alpha_j} + c_1 \frac{\mu_i^{\ 2}\alpha_j + \mu_j^{\ 2}\alpha_i}{\alpha_i\alpha_j} \quad (10)$$

where we consider c_0 and c_1 as coefficients to fit against the SAPT calculations. The distance r_{ij} is considered here to be the equilibrium distance of each dimer. Because we wish to test the predictive ability of this relation, we split the data set into a training and a test subsets, as shown in Figure 6, and we also applied a cross-validation procedure to detect an eventual bias in the choice of sets.

Regression using the training set yielded $c_0 = 0.25 \pm 0.02$ and $c_1 = 0.11 \pm 0.02$ for the coefficients of eq 10. Its ability to predict the k_{ij} factors from SAPT is illustrated in Figure 7a, where dimers are color-coded into four groups, depending on the charge of the monomers: cation−anion, cation−neutral, anion−neutral, and neutral−neutral. The agreement is overall good, with a standard deviation of 0.07 for the training set and 0.10 for the test set, which are equivalent in terms of scatter. In order to check if a bias was introduced by our choices of training and test sets, we carried out a cross-validation by refitting eq 10 for all the dimers leaving out each data point in turn (leave-one-out cross-validation[47]). The cross-validation did not reveal a significant bias arising from the choice of data sets.

The only systematic deviation apparent in Figure 7a occurs for dimers of neutral, nonpolar fragments, for which eq 10 predicts $k_{pred} = 1$. For such dimers, SAPT calculations give a small induction contribution, so $k_{SAPT} < 1$ with values roughly in the range 0.89−0.95. The deviations for dimers of nonpolar fragments are commensurate with the overall scatter of the fit but a systematic trend is observed nonetheless. We attempted to improve on this small systematic deviation by considering that, even if fragments are nonpolar, individual atoms can have significant partial charges, which give rise to induction effects. It could make sense to abandon the fragment approach when evaluating the first term in eq 10 and calculate it instead atom-by-atom

$$\sum_n^N \sum_m^M \frac{r_{mn}^{\ 2}(q_n^{\ 2}\alpha_m + q_m^{\ 2}\alpha_n)}{\alpha_m\alpha_n} \quad (11)$$

where N and M are the number of atoms in fragments i and j. This per-atom formula would require explicit interatomic distances r_{mn}, which depend on mutual orientations of the fragments. For simplicity, we replaced those by the distance between the centers of mass of the fragments, r_{ij}. The resulting fit is shown in Figure 7b. This per-atom approach indeed works better for dimers of nonpolar fragments, but for all the other classes, the fit is worse. Because the original deviations for the nonpolar dimers were small and because we are interested mainly in ionic systems, we considered the fragment-based scheme to be superior, which we will adopt.

Thus, we propose a fragment-based scheme to predict the scaling factors needed to upgrade a fixed-charge force field into a polarizable one. This scheme requires molecular quantities such as charge, permanent dipole moment, and polarizability, which have clear physical meaning and are simple to calculate using accessible quantum chemical methods.

Anticipating some of the results that will be discussed below, we found that introducing polarization explicitly in the force field and scaling the LJ terms lead to slightly lower densities for most ILs, when simulations are compared to experiments. This systematic deviation is on an average about −2%, a magnitude similar to the scatter observed for different ILs. Therefore, the maximum density deviations with respect to the experiment reach −4% for ILs we studied, as shown in Figure 8. We think that density is an essential property that affects the ability to

DOI: 10.1021/acs.jctc.9b00689
J. Chem. Theory Comput. XXXX, XXX, XXX−XXX

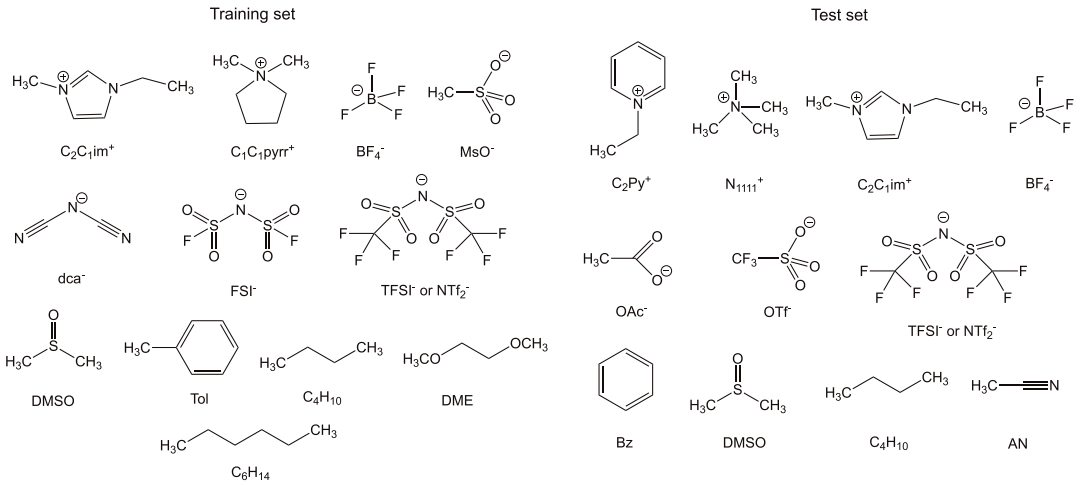

Figure 6. Fragments constituting the dimers in the training and test sets. Although some fragments are part of both sets, the dimers considered were different.

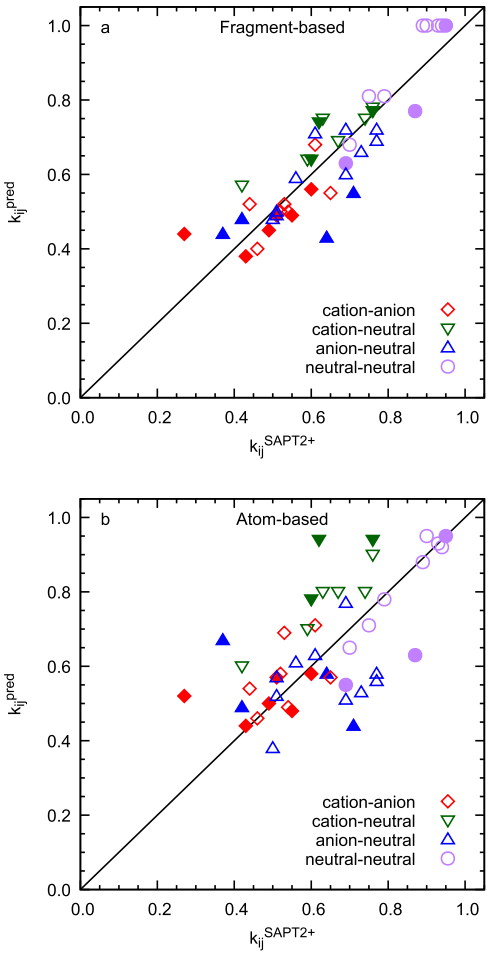

Figure 7. Predicted k_{ij} factors compared to values calculated from SAPT2+. Training set (empty points) and test set (filled points) obtained by the fragment-based (a) and atom-based (b) approaches.

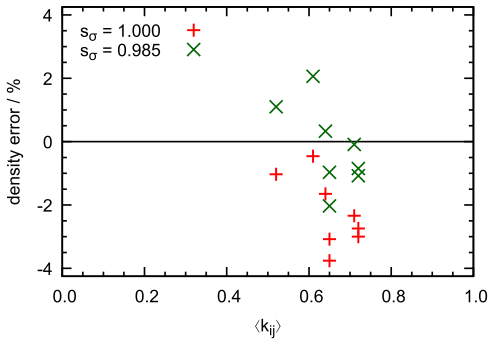

Figure 8. Density for several ILs calculated with the polarizable model, before and after correction of the σ parameter in the LJ interactions.

model, involves the following steps, which are illustrated in Figure 9: (1) adding Drude-induced dipoles derived from

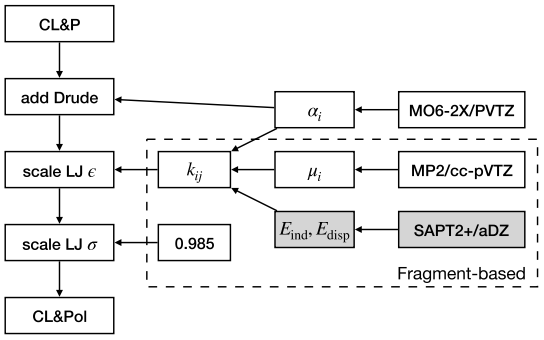

Figure 9. Block diagram illustrating the procedure leading to the CL&Pol force field. The blocks with gray background indicate the more expensive option to determine the k_{ij} scaling factors from SAPT calculations. Atomic polarizabilities α derived from quantum chemical calculations were obtained from the literature.[28]

predict many others, so we propose to improve the calculation of density by reducing the diameters of LJ sites, σ by 1.5% across the specification of the force field. This scaling of σ by a factor of 0.985 corrects the bias in liquid densities.

Our scheme to construct a polarizable force field for ILs and eutectic solvents, CL&Pol, starting from the fixed-charge CL&P atomic polarizabilities; (2) scaling down the well depth of der Waals interactions (LJ ϵ) by the appropriate k_{ij} factors, obtained either (a) from SAPT calculations on dimers (computationally expensive) or (b) from a general predictive scheme, which requires knowledge of atomic polarizabilities, fragment dipole moments, and dimer geometries from straightforward quantum

DOI: 10.1021/acs.jctc.9b00689
J. Chem. Theory Comput. XXXX, XXX, XXX−XXX

Table 3. Properties of ILs Calculated Using Different Force Fields[a]

	ρ/g cm^3	D_+/m^2 s^{-1}	D_-/m^2 s^{-1}	η/mPa s	ρ/g cm^3	D_+/m^2 s^{-1}	D_-/m^2 s^{-1}	η/mPa s
	[C_2C_1im][dca] 303 K				[C_4C_1im][Ntf_2] 323 K			
Exp	1.100	1.40×10^{-10}	1.50×10^{-10}	13.9	1.414	6.60×10^{-11}	5.20×10^{-11}	20.6
FixQ	1.102	1.43×10^{-11}	1.54×10^{-11}	362 ± 313	1.419	6.57×10^{-12}	4.67×10^{-12}	232 ± 43
ScaleQ	1.057	1.28×10^{-10}	1.46×10^{-10}	7.6 ± 1.6	1.385	4.62×10^{-11}	2.72×10^{-11}	54 ± 28
Drude	1.094	8.64×10^{-11}	1.09×10^{-10}	19 ± 5	1.414	2.74×10^{-11}	1.90×10^{-11}	58 ± 4
SDrude	1.095	1.62×10^{-10}	1.97×10^{-10}	8.6 ± 1.4	1.375	8.66×10^{-11}	7.86×10^{-11}	19 ± 7
CSDrude	1.123	1.66×10^{-10}	1.94×10^{-10}	7.6 ± 1.5	1.402	7.81×10^{-11}	6.27×10^{-11}	15 ± 7
KSDrude	1.093	1.53×10^{-10}	1.45×10^{-10}	8.7 ± 1.4	1.362	1.10×10^{-10}	1.06×10^{-10}	11 ± 2
KCSDrude *NpT*	1.122	1.48×10^{-10}	1.82×10^{-10}	8.4 ± 0.8	1.388	1.22×10^{-10}	1.19×10^{-10}	9.1 ± 1.6
KCSDrude *NVT*	1.121	1.72×10^{-10}	1.87×10^{-10}	8.4 ± 1.1	1.391	1.18×10^{-10}	1.05×10^{-10}	14 ± 4
	[C_2C_1im][BF_4] 323 K				[C_4C_1pyr][Ntf_2] 343 K			
Exp	1.264	1.05×10^{-10}	8.99×10^{-11}	17.4	1.355	1.02×10^{-10}	8.90×10^{-11}	16.2
FixQ	1.242	1.57×10^{-11}	4.25×10^{-12}	445 ± 228	1.360	2.88×10^{-12}	3.34×10^{-12}	554 ± 264
ScaleQ	1.175	1.59×10^{-10}	7.09×10^{-11}	20 ± 2	1.326	1.90×10^{-11}	1.47×10^{-11}	122 ± 91
Drude	1.228	5.53×10^{-11}	4.25×10^{-11}	88 ± 25	1.360	8.33×10^{-12}	7.96×10^{-12}	223 ± 182
SDrude	1.251	1.32×10^{-10}	9.38×10^{-11}	24 ± 14	1.304	6.19×10^{-11}	5.90×10^{-11}	19 ± 8
CSDrude	1.278	1.16×10^{-10}	8.68×10^{-11}	22 ± 5	1.328	7.36×10^{-11}	6.65×10^{-11}	15 ± 5
KCSDrude *NVT*	1.284	1.33×10^{-10}	1.09×10^{-10}	20 ± 7	1.323	8.31×10^{-11}	7.96×10^{-11}	8.7 ± 0.5
	[C_6C_1im][dca] 333 K				[C_4C_1pyr][dca] 323 K			
Exp	1.013	N/A	N/A	20.0	1.000	8.87×10^{-11}	1.16×10^{-10}	16.1
FixQ	1.017	1.07×10^{-11}	9.50×10^{-12}	208 ± 117	1.005	1.86×10^{-12}	1.54×10^{-12}	1061 ± 465
ScaleQ	0.984	8.44×10^{-11}	9.66×10^{-11}	13.1 ± 1.5	0.967	3.45×10^{-11}	4.93×10^{-11}	71 ± 48
Drude	1.009	3.36×10^{-11}	4.03×10^{-11}	35 ± 6	1.007	9.07×10^{-12}	1.09×10^{-11}	607 ± 382
SDrude	0.983	5.37×10^{-11}	8.76×10^{-11}	15 ± 3	0.983	3.21×10^{-11}	4.73×10^{-11}	23.2 ± 1.3
CSDrude	1.002	5.16×10^{-11}	8.34×10^{-11}	12.4 ± 1.2	1.003	5.21×10^{-11}	6.14×10^{-11}	36 ± 14
KCSDrude *NVT*	1.006	6.17×10^{-11}	9.82×10^{-11}	23 ± 7	1.006	5.57×10^{-11}	8.09×10^{-11}	31 ± 7
	[C_4C_1im][dca] 323 K				[C_4C_1im][BF_4] 343 K			
Exp	1.045	N/A	N/A	13.5	1.170	8.00×10^{-11}	8.20×10^{-11}	18.7
FixQ	1.049	2.12×10^{-11}	1.98×10^{-11}	122 ± 41	1.154	1.19×10^{-11}	8.82×10^{-12}	347 ± 82
Drude	1.039	7.75×10^{-11}	9.91×10^{-11}	23 ± 5	1.142	7.30×10^{-11}	5.79×10^{-11}	82 ± 40
SDrude	1.021	1.53×10^{-10}	2.05×10^{-10}	9.9 ± 0.7	1.134	9.29×10^{-11}	1.35×10^{-10}	19 ± 4
CSDrude	1.044	1.63×10^{-10}	2.02×10^{-10}	7.86 ± 0.15	1.159	1.17×10^{-10}	1.12×10^{-10}	12 ± 2
	[C_6C_1im][Ntf_2] 343 K				[C_6C_1im][BF_4] 353 K			
Exp	1.331	8.61×10^{-11}	8.12×10^{-11}	14.4	1.107	6.77×10^{-11}	7.02×10^{-11}	21.2
FixQ	1.340	1.03×10^{-11}	6.83×10^{-12}	384 ± 435	1.093	9.74×10^{-12}	6.70×10^{-12}	215 ± 59
Drude	1.336	2.87×10^{-11}	1.91×10^{-11}	42 ± 6	1.085	3.94×10^{-11}	4.07×10^{-11}	72 ± 40
SDrude	1.291	8.99×10^{-11}	1.01×10^{-10}	11 ± 4	1.067	4.44×10^{-11}	6.12×10^{-11}	26 ± 6
	[C_2C_1im][Ntf_2] 323 K							
Exp	1.493	1.12×10^{-10}	7.54×10^{-11}	15.6				
FixQ	1.494	7.49×10^{-12}	4.07×10^{-12}	101 ± 27				
Drude	1.488	3.58×10^{-11}	2.33×10^{-11}	68 ± 32				
SDrude	1.458	1.09×10^{-10}	5.89×10^{-11}	12 ± 3				

[a]FixQ: fixed-charge CL&P force field; ScaleQ: FixQ model with scaled charges by 0.8; Drude: FixQ model with polarization added; SDrude: Drude model with scaled LJ ϵ by k_{ij}^{SAPT2+}; CSDrude: SDrude model with scaled LJ σ by 0.985; KSDrude: Drude model with scaled LJ ϵ by k_{ij}^{pred}; KCSDrude: KSDrude model with scaled LJ σ by 0.985. Experimental values of density, ion diffusion coefficients, and viscosity from the literature.

chemical methods; and (3) correcting the density by scaling down atomic diameters (LJ σ) by 0.985.

6. CALCULATION OF EQUILIBRIUM AND TRANSPORT PROPERTIES

Structural and dynamic quantities are among the most important ones that are studied by MD simulations of ILs because the absence of volatility of these fluids complicates the study of energetic properties (vapor pressure is one of the keys leading to cohesive energy and chemical potential in organic liquids). In our previous study,[8] we discussed the influence of Drude-induced dipoles and of the scaling of the LJ potential on the density, local structure, coordination numbers, and diffusion coefficients of some ILs. Here, we extend the analysis to a much larger data set and with the following force field settings:

1. FixQ: fixed-charge CL&P force field;
2. ScaleQ: FixQ model with scaled charges by 0.8;
3. Drude: polarization added to FixQ model;
4. SDrude: Drude model with scaled ϵ_{ij} LJ by k_{ij}^{SAPT2+};
5. CSDrude: SDrude model with scaled LJ σ_{ij} by 0.985;
6. KSDrude: Drude model with scaled LJ ϵ_{ij} by k_{ij}^{pred};
7. KCSDrude: KSDrude model with scaled LJ σ_{ij} by 0.985.

The results for several representative ILs, including different cation and anion head groups, and several lengths of alkyl chains, are given in Table 3, together with experimental data from the literature.[48−60] Some of the simulations with our final version of force field, KCSDrude, were performed both in the *NpT* and

DOI: 10.1021/acs.jctc.9b00689
J. Chem. Theory Comput. XXXX, XXX, XXX−XXX

Table 4. Properties of Ethylmethylimidazolium Acetate and Its Mixture with DMSO Calculated Using Different Force Field Settings[a]

	ρ/g cm^3	D_+/m^2 s^{-1}	D_-/m^2 s^{-1}	η/mPa s	ρ/g cm^3	D_+/m^2 s^{-1}	D_-/m^2 s^{-1}	D_{solv}/m^2 s^{-1}	η/mPa s
	[C_2C_1im][OAc] 298 K				[C_2C_1im][OAc]−DMSO (f_{DMSO} = 0.4) 298 K				
Exp	1.107	9.52×10^{-12}	7.95×10^{-12}	115−144	1.104	5.41×10^{-11}	5.35×10^{-11}	1.53×10^{-10}	16.3
FixQ	1.114	1.08×10^{-12}	6.44×10^{-13}	1659 ± 1291	1.115	4.64×10^{-12}	2.53×10^{-12}	1.23×10^{-11}	609 ± 417
KCSDrude	1.147	5.14×10^{-11}	5.26×10^{-11}	67 ± 20	1.119	4.96×10^{-10}	4.90×10^{-11}	2.37×10^{-10}	14.1 ± 1.3

[a]FixQ: fixed-charge CL&P force field; KCSDrude: FixQ model with added polarization, scaled LJ ϵ by k_{ij}^{pred} and scaled LJ σ by 0.985. Experimental values taken from the literature.

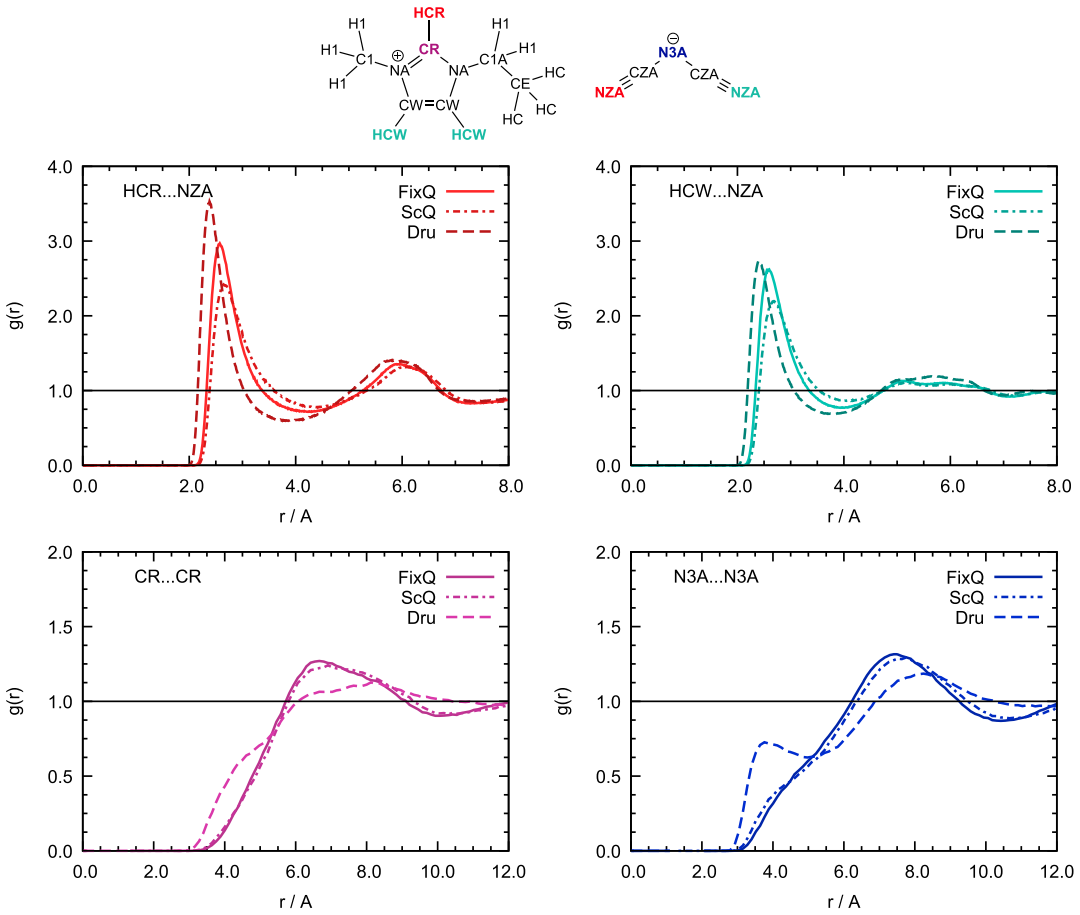

Figure 10. Radial distribution function between representative atoms of the cation and anion of [C_2C_1im][dca] obtained with the FixQ, ScaleQ, and KCSDrude force fields.

NVT ensembles to check if thermostats and barostats were introducing any artifacts into the calculated quantities (none found).

The general trends in calculated properties are discussed herein. While the density values obtained from the fixed-charge CL&P force field are in good agreement with the experiment, the transport properties suffer from slow dynamics, with diffusion coefficients that are too low and viscosities that are too high, by 1 order of magnitude or more, as expected. We report the results using scaled-down ionic charges by 0.8 for six ILs. The scaled-charge nonpolarizable force field leads to much improved dynamics in the four imidazolium ILs we tested and also improved dynamics but not up to quantitative agreement for the two pyrrolidinium ILs we studied. Scaling-down charges has a big negative impact on densities, leading to underestimations between −2.4 and −7.0% from experimental values, which is comparable to what other authors have also found.[11]

When Drude polarization is introduced, a decrease in density of ca. 1% is observed in the majority of liquids, becoming more accentuated when the ϵ are scaled. Exceptions are pyrrolidinium ILs, for which we do not see such density changes, and [C_2C_1im][BF_4], whose density increases slightly. Scaling σ as proposed above improves the agreement with experimental densities overall, which is within ±2% for the polarizable force field in versions CSDrude and KCSDrude. There are no significant differences in the agreement of densities between using k_{ij} values from SAPT and from our predictive scheme.

Adding polarization to the CL&P force field decreases the calculated viscosity and increases the simulated diffusion coefficients by 1 order of magnitude, leading to immensely improved predictions of dynamic quantities. Scaling the ϵ further fluidifies the systems, improving even more the prediction of transport properties. The small correction to σ aimed at improving density has negligible effects on the

DOI: 10.1021/acs.jctc.9b00689
J. Chem. Theory Comput. XXXX, XXX, XXX−XXX

calculated transport properties that agree within the statistical errors.

The use of k_{ij} scaling factors from SAPT or from our predictive scheme also lead to similar values for the calculated properties, validating the different choices and approximations made when formulating this scheme.

We made similar comparisons of density and predicted transport properties for a mixture of an IL with a molecular solvent, $[C_2C_1im][OAc]$ + DMSO, with mole fraction of x_{DMSO} = 0.4. The simulations were done using the FixQ and KCSDrude force field settings. Results and comparisons with literature data[58,61−64] are given in Table 4.

The predicted density with the polarizable force field for the pure IL are slightly higher than the experimental value, whereas the predicted dynamics are slightly too fast (larger diffusivities and lower viscosities than experimental). It should be noted that $[C_2C_1im][OAc]$ is a highly hygroscopic, slightly protic IL, which may cause experimental errors, mainly because of uncontrolled water content. Proton transfer is expected to be too low to affect the results. In spite of these deviations on the pure IL, the polarizable force field predicts remarkably well the properties of the mixture with the molecular compound.

The CL&Pol force field presented here has comparable performance to two other polarizable force fields from the literature: the APPLE&P force field developed by Borodin et al.[20] for several families of cations and anions predicts densities within ±1% and transport properties within roughly a factor of 1.5−2. The polarizable force field developed Yethiraj et al.[65,66] for imidazolium ILs with several anions predicting densities within −3.7 and 2.3% and transport properties within approximately a factor of 1.5. The CL&Pol force field is more easily extendable to many families of ILs because it is fragment-based and the predictive scheme for scale factors is computationally simple. It is also more easily combined with compounds and materials described by force fields with functional forms based on LJ plus Coulomb potentials, which represent the vast majority.

It is interesting to investigate the origin of the improved (faster) dynamics upon introduction of polarization because the induction terms added should be attractive (at least in a pairwise case). Analysis of radial and spatial distribution functions between atomic sites showed some changes to the first-neighbor shells with slightly more intense first peaks appearing at shorter distances, as shown in Figure 10. This indicates stronger attraction between immediate neighbors, as expected. On the contrary, the second-shell features in the radial distribution functions are less pronounced with the polarizable model, indicating that longer-range ordering is less marked, as seen in the iso-density contours in spatial distribution functions, shown in Figure 11. The faster dynamics obtained with the polarizable force field are likely to be a consequence of weaker long-range correlations, without disruption of first-shell structure.

Using scaled-down charges with a nonpolarizable force field leads to first-neighbor peaks that have lower intensity and are displaced to longer distances (related to the lower densities obtained). Polarizable force fields represent interactions more faithfully, when compared to the simply scaling down ionic charges used to improve dynamics in fixed-charge models, as has been pointed out by several authors.[12,13]

7. CONCLUSIONS

We propose a transferable, general, polarizable force field for ILs and their mixtures with molecular compounds (including eutectic solvents), CL&Pol, that is a result of upgrading the widely used CL&P fixed-charge force field. A fragment-based approach was followed such that parameters for many molecular structures can be generated with ease. These two choices avoid extensive reparametrization, allowing to cover a wide variety of cation and anion structures. Exploring a multitude of molecular structures and functional groups is one of the most relevant and interesting features of research in ILs, aimed at choosing and designing alternative solvents and technological fluids.

The upgrade of the fixed-charge CL&P force field requires scaling of the LJ parameters to compensate for the addition of explicit polarization in the form of Drude-induced dipoles. The scaling of the LJ terms can be based on directly calculated factors, obtained from SAPT quantum calculations, which are expensive computationally (a few days on 16 processors). We developed an alternative predictive scheme for the scaling factors using only simple quantities such as dipole moment, polarizability, and total charge of the interacting molecular fragments. This predictive scheme was validated through calculation of density, ion diffusion coefficients, and viscosity for 12 ILs and one mixture with a molecular compound. Comparison with experiment showed much improved predictions of transport properties, which was a serious shortcoming of the fixed-charge model. Also, including polarization explicitly in the force field leads to much better performance than scaling-down charges in the CL&P model, as the scaled-charge force field underestimates liquid densities severely and still overestimates transport properties for pyrrolidinium ILs.

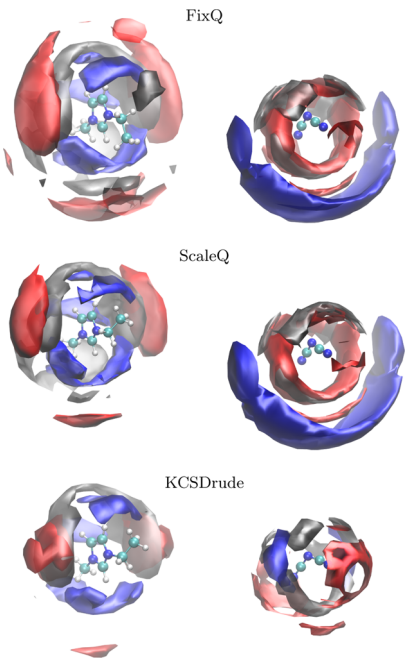

Figure 11. Spatial distribution functions of selected atoms around the cation (left) and the anion (right) in $[C_2C_1im][dca]$ for FixQ (top), ScaleQ (center), and KCSDrude (bottom) force field settings. The blue surface corresponds to NZA atoms of anions (isodensity contours at 4 and 1.4 times the average density around the cation and the anion, respectively), the red surface to CR atoms of cations (isodensity contours at 1.5 and 2.3 times the average density around the cation and the anion, respectively), and the gray surface to CE atoms of cation alkyl chains (isodensity contours at 1.5 and 2.7 times the average density around the cation and the anion, respectively). The second-shell structure (cation−cation and anion−anion) is less marked with the polarizable model.

DOI: 10.1021/acs.jctc.9b00689
J. Chem. Theory Comput. XXXX, XXX, XXX−XXX

Table 5. Induction and Dispersion Contributions, and Fraction of Dispersion in Non-Coulomb Attraction, k_{ij}, Obtained with Different SAPT Levels and by the Present Predictive Scheme, for the Dimers of Fragments Considered in This Work[a]

dimer	E_{tot}^{sSAPT0}	E_{ind}^{sSAPT0}	E_{disp}^{sSAPT0}	k_{ij}^{sSAPT0}	E_{tot}^{SAPT2+}	E_{ind}^{SAPT2+}	E_{disp}^{SAPT2+}	k_{ij}^{SAPT2+}	k_{ij}^{pred}
Cation−Anion									
$C_2C_1im^+\cdots dca^-$	−358.6	−35.2	−52.9	0.60	−368.0	−40.8	−63.8	0.61	0.68
$C_2C_1im^+\cdots Ntf_2^-$	−348.1	−29.8	−51.9	0.64	−362.1	−38.5	−72.3	0.65	0.55
$C_2C_1im^+\cdots BF_4^-$	−355.2	−34.9	−28.1	0.45	−368.4	−42.7	−46.3	0.52	0.50
$C_2C_1im^+\cdots MsO^-$	−415.8	−59.8	−36.5	0.38	−422.2	−72.4	−56.1	0.44	0.52
$C_2C_1im^+\cdots OAc^-$	−465.5	−151.8	−43.0	0.22	−465.2	−177.3	−64.1	0.27	0.44
$C_2C_1im^+\cdots OTf^-$	−362.8	−44.9	−36.2	0.45	−375.9	−56.5	−54.7	0.49	0.45
$C_1C_1pyrr^+\cdots dca^-$	−338.6	−33.0	−34.1	0.51	−349.6	−38.2	−42.9	0.53	0.52
$C_1C_1pyrr^+\cdots Ntf_2^-$	−332.7	−40.2	−38.8	0.49	−342.9	−48.1	−55.7	0.54	0.50
$C_1C_1pyrr^+\cdots BF_4^-$	−361.0	−40.2	−24.3	0.38	−375.3	−49.1	−41.3	0.46	0.40
$C_2Py^+\cdots BF_4^-$	−358.2	−35.1	−28.6	0.45	−373.6	−43.5	−45.9	0.51	0.49
$C_2Py^+\cdots Ntf_2^-$	−342.5	−37.0	−48.5	0.57	−353.2	−44.9	−66.1	0.60	0.56
$N_{1111}^+\cdots BF_4^-$	−358.1	−37.0	−20.0	0.35	−372.1	−45.6	−34.6	0.43	0.38
$N_{1111}^+\cdots Ntf_2^-$	−334.4	−34.7	−36.6	0.51	−349.9	−44.1	−53.1	0.55	0.49
Cation−Neutral									
$C_2C_1im^+\cdots C_4H_{10}$	−19.8	−9.2	−27.6	0.75	−24.7	−10.3	−33.2	0.76	0.78
$C_2C_1im^+\cdots C_6H_{14}$	−23.0	−10.8	−28.6	0.73	−29.2	−12.5	−34.9	0.74	0.75
$C_2C_1im^+\cdots Bz$	−49.3	−22.2	−33.6	0.60	−47.7	−23.5	−37.8	0.62	0.74
$C_2C_1im^+\cdots Tol$	−54.5	−28.4	−45.4	0.61	−53.9	−26.6	−44.7	0.63	0.75
$C_2C_1im^+\cdots DMSO$	−105.1	−36.1	−19.9	0.36	−88.2	−39.1	−28.4	0.42	0.57
$C_1C_1pyrr^+\cdots C_4H_{10}$	−13.2	−8.4	−15.0	0.64	−17.6	−10.6	−21.8	0.67	0.69
$C_1C_1pyrr^+\cdots DME$	−47.5	−14.2	−17.8	0.56	−47.0	−16.5	−24.2	0.59	0.64
$C_2Py^+\cdots C_4H_{10}$	−17.7	−7.8	−23.6	0.75	−21.3	−8.8	−27.3	0.76	0.77
$N_{1111}^+\cdots C_4H_{10}$	−12.7	−10.7	−14.4	0.57	−17.0	−12.1	−18.6	0.60	0.64
Anion−Neutral									
$C_4H_{10}\cdots dca^-$	−18.0	−9.6	−17.2	0.64	−25.6	−12.2	−26.8	0.69	0.72
$C_4H_{14}\cdots dca^-$	−25.1	−16.7	−21.8	0.57	−32.9	−18.4	−28.9	0.61	0.71
$C_4H_{10}\cdots Ntf_2^-$	−17.2	−9.2	−17.5	0.65	−25.0	−10.5	−26.1	0.77	0.69
$C_6H_{14}\cdots Ntf_2^-$	−26.5	−13.3	−25.2	0.65	−30.3	−10.4	−34.4	0.77	0.72
$C_4H_{10}\cdots BF_4^-$	−20.0	−16.6	−11.2	0.40	−28.8	−19.1	−20.2	0.51	0.49
$C_6H_{14}\cdots BF_4^-$	−26.1	−20.8	−13.9	0.40	−36.4	−23.7	−24.7	0.51	0.50
$C_4H_{10}\cdots MsO^-$	−28.3	−20.6	−18.3	0.47	−37.2	−23.1	−29.3	0.56	0.59
$DMSO\cdots Ntf_2^-$	−53.5	−12.4	−23.3	0.65	−58.0	−15.0	−34.0	0.69	0.60
$DMSO\cdots OAc^-$	−97.8	−39.5	−21.2	0.35	−102.1	−49.3	−35.9	0.42	0.48
$DME\cdots FSI^-$	−25.8	−7.5	−16.5	0.69	−34.1	−9.8	−26.7	0.73	0.66
$Tol\cdots MsO^-$	−38.0	−26.5	−19.7	0.43	−44.8	−30.1	−30.6	0.50	0.48
$AN\cdots Ntf_2^-$	−35.7	−6.0	−11.1	0.65	−38.9	−7.0	−17.1	0.71	0.55
$Bz\cdots OAc^-$	−50.0	−41.4	−16.5	0.29	−55.0	−46.6	−27.5	0.37	0.44
$Bz\cdots OTf^-$	−10.0	−4.5	−5.9	0.57	−14.5	−5.5	−9.9	0.64	0.43
Neutral−Neutral									
$C_4H_{10}\cdots C_4H_{10}$	−5.5	−0.60	−9.3	0.94	−8.2	−0.89	−14.1	0.94	1.00
$C_4H_{10}\cdots Tol$	−15.4	−2.9	−27.8	0.91	−16.6	−5.0	−43.1	0.90	1.00
$DMSO\cdots DMSO$	−33.9	−11.5	−20.4	0.64	−34.4	−13.1	−30.6	0.70	0.68
$DMSO\cdots Tol$	−25.2	−10.3	−25.4	0.71	−26.5	−11.2	−33.9	0.75	0.81
$DMSO\cdots C_4H_{10}$	−11.2	−6.0	−16.0	0.73	−15.8	−6.3	−23.2	0.79	0.81
$DME\cdots DME$	−14.0	−3.0	−18.5	0.86	−19.6	−3.4	−26.6	0.89	1.00
$DME\cdots C_4H_{10}$	−9.7	−1.6	−15.9	0.91	−14.2	−1.7	−21.6	0.93	1.00
$AN\cdots C_4H_{10}$	−6.0	−1.5	−9.0	0.86	−8.6	−1.7	−11.9	0.87	0.77
$AN\cdots AN$	−26.6	−5.8	−10.9	0.65	−25.3	−7.2	−16.2	0.69	0.63
$Bz\cdots Bz$	−5.7	−1.1	−21.2	0.95	−8.1	−1.1	−21.6	0.95	1.00

[a]Energies are given in $kJ\cdot mol^{-1}$.

Analysis of the microscopic structure of the ILs shows that the structure between the first-neighbors is not disrupted, but the second-shell structural features, between ions of the same charge, are considerably weaker when polarization is included explicitly. The faster dynamics obtained with the polarizable force field are thus linked to this loss of second-shell structure.

Parameters and scripts to prepare input files using the CL&Pol force field are made available in code repositories.[40]

APPENDIX

Evaluation of Induction and Dispersion Energies

Detailed values of quantities and contributions calculated with different SAPT levels are collected in Table 5. Energetic

DOI: 10.1021/acs.jctc.9b00689
J. Chem. Theory Comput. XXXX, XXX, XXX−XXX

Table 6. Energy Averages from MD Trajectories Corresponding to LJ and Electrostatic Contributions for ILs and Isolated Ions, Used To Calculate Cohesive Energies[a]

$(E/\mathrm{kJ\cdot mol^{-1}})$	$\frac{\langle E^{IL}\rangle}{N}$	$\frac{\langle E^{IL}_{LJ}\rangle}{N}$	$\frac{\langle E^{IL}_{elst}\rangle}{N}$	$\langle E^{+}\rangle$	$\langle E_{LJ}{}^{+}\rangle$	$\langle E_{elst}{}^{+}\rangle$	$\langle E^{-}\rangle$	$\langle E_{LJ}{}^{-}\rangle$	$\langle E_{elst}{}^{-}\rangle$
$[C_4C_1im][BF_4]$ 343 K									
FixQ	−153.7	−63.5	−283.9	306.2	−1.3	150.5	22.8	0.0	0.0
Drude	−159.5	−60.8	−308.3	240.3	−2.2	125.5	23.1	0.0	0.0
SDrude	−143.7	−36.3	−319.1	238.3	−1.8	125.3	23.1	0.0	0.0
$[C_2C_1im][dca]$ 303 K									
FixQ	−244.8	−73.6	−304.7	240.3	−1.1	141.7	7.0	−0.50	−16.8
Drude	−254.9	−69.9	−348.8	244.2	−0.98	139.3	−0.61	−0.56	−26.3
SDrude	−240.5	−48.4	−360.6	244.2	−0.98	139.3	−0.61	−0.56	−26.3
$[C_4C_1im][Ntf_2]$ 323 K									
FixQ	122.9	−119.5	−26.1	295.3	−1.5	150.5	307.2	−0.45	193.5
Drude	103.5	−116.4	−83.5	234.2	−2.1	125.5	288.4	0.35	152.3
SDrude	137.0	−80.8	−87.2	234.0	−1.7	125.4	288.4	0.35	152.3
$[C_4C_1pyr][Ntf_2]$343 K									
FixQ	317.5	−91.5	20.9	478.1	23.4	195.3	314.5	−0.31	194.2
Drude	295.0	−89.0	−38.7	413.1	19.1	159.1	294.7	0.38	153.1
SDrude	338.0	−44.7	−41.1	406.3	19.8	159.3	294.7	0.38	153.1
$[C_4C_1im][dca]$ 323 K									
FixQ	−190.0	−81.9	−288.7	295.3	−1.5	150.5	8.2	−0.51	−16.7
Drude	−201.8	−77.4	−340.7	234.2	−2.1	125.5	0.37	−0.56	−26.3
SDrude	−182.5	−50.4	−354.5	234.0	−1.7	125.4	0.37	−0.56	−26.3
$[C_4C_1pyr][dca]$ 323 K									
FixQ	−14.1	−57.1	−241.1	471.1	23.2	195.1	8.2	−0.51	−16.7
Drude	−28.1	−55.1	−286.6	400.2	18.4	159.2	0.37	−0.56	−26.3
SDrude	−3.3	−25.1	−295.3	410.3	19.4	159.7	0.37	−0.56	−26.3
$[C_6C_1im][dca]$ 323 K									
FixQ	−154.2	−91.2	−282.9	339.7	−0.84	153.3	8.2	−0.51	−16.7
Drude	−167.7	−86.6	−340.4	270.1	−2.0	115.7	0.37	−0.56	−26.3
SDrude	−147.6	−56.9	−357.2	271.3	−1.4	115.6	0.37	−0.56	−26.3
$[C_2C_1im][Ntf_2]$ 323 K									
FixQ	82.1	−109.8	−38.2	249.1	−0.94	141.8	307.2	−0.45	193.5
Drude	63.2	−106.8	−93.0	247.9	−0.92	139.4	288.4	0.35	152.3
SDrude	93.7	−74.8	−96.3	247.9	−0.92	139.4	288.4	0.35	152.3
$[C_6C_1im][Ntf_2]$ 343 K									
FixQ	181.0	−125.3	−19.9	348.8	−0.78	153.0	314.5	−0.31	194.2
Drude	160.9	−122.2	−80.0	276.2	−2.1	115.5	294.7	0.38	153.1
SDrude	196.5	−84.4	−83.8	279.0	−1.3	115.4	294.7	0.38	153.1
$[C_2C_1im][BF_4]$ 323 K									
FixQ	−212.3	−55.7	−300.5	249.1	−0.94	141.8	22.4	0.0	0.0
Drude	−216.7	−53.5	−319.3	247.9	−0.92	139.4	21.8	0.0	0.0
SDrude	−206.7	−35.4	−328.7	247.9	−0.92	139.4	21.8	0.0	0.0
$[C_6C_1im][BF_4]$ 353 K									
FixQ	−106.6	−71.0	−277.9	354.7	−0.50	153.3	23.9	0.0	0.0
Drude	−140.1	−71.7	−308.7	281.7	−1.9	115.4	23.3	0.0	0.0
SDrude	−124.4	−45.3	−322.0	281.2	−1.4	115.4	23.3	0.0	0.0

[a]FixQ: fixed-charge CL&P force field; Drude: CL&P model with polarization added; SDrude: Drude model with scaled LJ ϵ by k_{ij}^{SAPT2+}. Note the 0 values for BF_4^- because intramolecular interactions are excluded in the force field (there are no atoms separated by more than two bonds).

quantities averaged from MD trajectories for the ILs studied here, decomposed into LJ and electrostatic terms for cations and anions, are collected in Table 6.

AUTHOR INFORMATION

Corresponding Author

*E-mail: agilio.padua@ens-lyon.fr.

ORCID

Kateryna Goloviznina: 0000-0001-9913-4938
José N. Canongia Lopes: 0000-0002-4483-6294
Margarida Costa Gomes: 0000-0001-8637-6057
Agílio A. H. Pádua: 0000-0002-7641-6526

Notes

The authors declare no competing financial interest.

ACKNOWLEDGMENTS

The authors thank Prof. Tatiana Budtova (U. Nice, France) and Dr. Michael E. Ries (U. Leeds, UK) for supplying the raw data of transport properties of $[C_2C_1im][OAc]$ + DMSO and thank Dr. Carlos Bernardes (U. Lisbon, Portugal) for discussions

DOI: 10.1021/acs.jctc.9b00689
J. Chem. Theory Comput. XXXX, XXX, XXX−XXX

concerning the polarizable model. This work was supported by an IDEX Lyon Fellowship (ANR-16-IDEX-005). Electronic structure calculations and MD simulations were performed on the computer clusters of the Pôle Scientifique de Modélisation Numérique (PSMN) at ENS de Lyon.

REFERENCES

(1) Plechkova, N. V.; Seddon, K. R. Applications of ionic liquids in the chemical industry. *Chem. Soc. Rev.* **2008**, *37*, 123.
(2) *Ionic Liquids in Synthesis*; Wasserscheid, P., Welton, T., Eds.; Wiley, 2003, p 380.
(3) Canongia Lopes, J. N.; Deschamps, J.; Pádua, A. A. H. Modeling Ionic Liquids Using a Systematic All-Atom Force Field. *J. Phys. Chem. B* **2004**, *108*, 2038.
(4) Sambasivarao, S. V.; Acevedo, O. Development of OPLS-AA Force Field Parameters for 68 Unique Ionic Liquids. *J. Chem. Theory Comput.* **2009**, *5*, 1038.
(5) Canongia Lopes, J. N.; Pádua, A. A. H. CL&P: A generic and systematic force field for ionic liquids modeling. *Theor. Chem. Acc.* **2012**, *131*, 1129.
(6) Jorgensen, W. L.; Maxwell, D. S.; Tirado-Rives, J. Development and Testing of the OPLS All-Atom Force Field on Conformational Energetics and Properties of Organic Liquids. *J. Am. Chem. Soc.* **1996**, *118*, 11225.
(7) Wang, J.; Wolf, R. M.; Caldwell, J. W.; Kollman, P. A.; Case, D. A. Development and testing of a general amber force field. *J. Comp. Chem.* **2004**, *25*, 1157.
(8) Pádua, A. A. H. Resolving dispersion and induction components for polarisable molecular simulations of ionic liquids. *J. Chem. Phys.* **2017**, *146*, 204501.
(9) Bhargava, B. L.; Balasubramanian, S. Refined potential model for atomistic simulations of ionic liquid [bmim][PF6]. *J. Chem. Phys.* **2007**, *127*, 114510.
(10) Chaban, V. Polarizability versus mobility: atomistic force field for ionic liquids. *Phys. Chem. Chem. Phys.* **2011**, *13*, 16055.
(11) Zhang, Y.; Maginn, E. J. A Simple AIMD Approach to Derive Atomic Charges for Condensed Phase Simulation of Ionic Liquids. *J. Phys. Chem. B* **2012**, *116*, 10036.
(12) Schröder, C. Comparing reduced partial charge models with polarizable simulations of ionic liquids. *Phys. Chem. Chem. Phys.* **2012**, *14*, 3089.
(13) McDaniel, J. G.; Yethiraj, A. Influence of Electronic Polarization on the Structure of Ionic Liquids. *J. Phys. Chem. Lett.* **2018**, *9*, 4765.
(14) Lamoureux, G.; Roux, B. Modeling induced polarization with classical Drude oscillators: Theory and molecular dynamics simulation algorithm. *J. Chem. Phys.* **2003**, *119*, 3025.
(15) Patel, S.; Brooks, C. L., III CHARMM fluctuating charge force field for proteins: I parameterization and application to bulk organic liquid simulations. *J. Comput. Chem.* **2004**, *25*, 1.
(16) Ponder, J. W.; Wu, C.; Ren, P.; Pande, V. S.; Chodera, J. D.; Schnieders, M. J.; Haque, I.; Mobley, D. L.; Lambrecht, D. S.; DiStasio, R. A.; Head-Gordon, M.; Clark, G. N. I.; Johnson, M. E.; Head-Gordon, T. Current Status of the AMOEBA Polarizable Force Field. *J. Phys. Chem. B* **2010**, *114*, 2549.
(17) Wang, J.; Cieplak, P.; Li, J.; Wang, J.; Cai, Q.; Hsieh, M.; Lei, H.; Luo, R.; Duan, Y. Development of Polarizable Models for Molecular Mechanical Calculations II: Induced Dipole Models Significantly Improve Accuracy of Intermolecular Interaction Energies. *J. Phys. Chem. B* **2011**, *115*, 3100.
(18) Jing, Z.; Liu, C.; Cheng, S. Y.; Qi, R.; Walker, B. D.; Piquemal, J.-P.; Ren, P. Polarizable Force Fields for Biomolecular Simulations: Recent Advances and Applications. *Annu. Rev. Biophys.* **2019**, *48*, 371.
(19) Yan, T.; Wang, Y.; Knox, C. On the Structure of Ionic Liquids: Comparisons between Electronically Polarizable and Nonpolarizable Models I. *J. Phys. Chem. B* **2010**, *114*, 6905.
(20) Borodin, O. Polarizable Force Field Development and Molecular Dynamics Simulations of Ionic Liquids. *J. Phys. Chem. B* **2009**, *113*, 11463.
(21) Salanne, M. Simulations of room temperature ionic liquids: from polarizable to coarse-grained force fields. *Phys. Chem. Chem. Phys.* **2015**, *17*, 14270.
(22) Bedrov, D.; Piquemal, J.-P.; Borodin, O.; MacKerell, A. D.; Roux, B.; Schröder, C. Molecular Dynamics Simulations of Ionic Liquids and Electrolytes Using Polarizable Force Fields. *Chem. Rev.* **2019**, *119*, 7940.
(23) Jiang, W.; Hardy, D. J.; Phillips, J. C.; MacKerell, A. D.; Schulten, K.; Roux, B. High-Performance Scalable Molecular Dynamics Simulations of a Polarizable Force Field Based on Classical Drude Oscillators in NAMD. *J. Phys. Chem. Lett.* **2011**, *2*, 87.
(24) Dequidt, A.; Devémy, J.; Pádua, A. A. H. Thermalized Drude Oscillators with the LAMMPS Molecular Dynamics Simulator. *J. Chem. Info. Model* **2016**, *56*, 260.
(25) Lemkul, J. A.; Roux, B.; van der Spoel, D.; MacKerell, A. D., Jr. Implementation of extended Lagrangian dynamics in GROMACS for polarizable simulations using the classical Drude oscillator model. *J. Comp. Chem.* **2015**, *36*, 1473.
(26) Huang, J.; Lemkul, J. A.; Eastman, P. K.; MacKerell, A. D., Jr. Molecular dynamics simulations using the drude polarizable force field on GPUs with OpenMM: Implementation, validation, and benchmarks. *J. Comput. Chem.* **2018**, *39*, 1682.
(27) Bernardes, C. E. S.; Shimizu, K.; Canongia Lopes, J. N.; Marquetand, P.; Heid, E.; Steinhauser, O.; Schröder, C. Additive polarizabilities in ionic liquids. *Phys. Chem. Chem. Phys.* **2016**, *18*, 1665.
(28) Heid, E.; Szabadi, A.; Schröder, C. Quantum mechanical determination of atomic polarizabilities of ionic liquids. *Phys. Chem. Chem. Phys.* **2018**, *20*, 10992.
(29) Jeziorski, B.; Moszynski, R.; Szalewicz, K. Perturbation Theory Approach to Intermolecular Potential Energy Surfaces of van der Waals Complexes. *Chem. Rev.* **1994**, *94*, 1887.
(30) Hohenstein, E. G.; Sherrill, C. D. Wavefunction methods for noncovalent interactions. *Wiley Interdiscip. Rev. Comput. Mol. Sci* **2011**, *2*, 304.
(31) Canongia Lopes, J. N.; Pádua, A. A. H.; Shimizu, K. Molecular Force Field for Ionic Liquids IV: Trialkylimidazolium and Alkoxycarbonyl-Imidazolium Cations; Alkylsulfonate and Alkylsulfate Anions. *J. Phys. Chem. B* **2008**, *112*, 5039.
(32) Grimme, S.; Antony, J.; Ehrlich, S.; Krieg, H. A consistent and accurate ab initio parametrization of density functional dispersion correction (DFT-D) for the 94 elements H-Pu. *J. Chem. Phys.* **2010**, *132*, 154104.
(33) Parker, T. M.; Burns, L. A.; Parrish, R. M.; Ryno, A. G.; Sherrill, C. D. Levels of symmetry adapted perturbation theory (SAPT). I. Efficiency and performance for interaction energies. *J. Chem. Phys.* **2014**, *140*, 094106.
(34) Turney, J. M.; Simmonett, A. C.; Parrish, R. M.; Hohenstein, E. G.; Evangelista, F. A.; Fermann, J. T.; Mintz, B. J.; Burns, L. A.; Wilke, J. J.; Abrams, M. L.; Russ, N. J.; Leininger, M. L.; Janssen, C. L.; Seidl, E. T.; Allen, W. D.; Schaefer, H. F.; King, R. A.; Valeev, E. F.; Sherrill, C. D.; Crawford, T. D. Psi4: an open-source ab initio electronic structure program. *WIREs: Comp. Mol. Sci.* **2012**, *2*, 556.
(35) Frisch, M. J.; Trucks, G. W.; Schlegel, H. B.; Scuseria, G. E.; Robb, M. A.; Cheeseman, J. R.; Scalmani, G.; Barone, V.; Petersson, G. A.; Nakatsuji, H.; Li, X.; Caricato, M.; Marenich, A. V.; Bloino, J.; Janesko, B. G.; Gomperts, R.; Mennucci, B.; Hratchian, H. P.; Ortiz, J. V.; Izmaylov, A. F.; Sonnenberg, J. L.; Williams-Young, D.; Ding, F.; Lipparini, F.; Egidi, F.; Goings, J.; Peng, B.; Petron, A.; Henderson, T.; Ranasinghe, D.; Zakrzewski, V. G.; Gao, J.; Rega, N.; Zheng, G.; Liang, W.; Hada, M.; Ehara, M.; Toyota, K.; Fukuda, R.; Hasegawa, J.; Ishida, M.; Nakajima, T.; Honda, Y.; Kitao, O.; Nakai, H.; Vreven, T.; Throssell, K.; Montgomery, J. A., Jr.; Peralta, J. E.; Ogliaro, F.; Bearpark, M. J.; Heyd, J. J.; Brothers, E. N.; Kudin, K. N.; Staroverov, V. N.; Keith, T. A.; Kobayashi, R.; Normand, J.; Raghavachari, K.; Rendell, A. P.; Burant, J. C.; Iyengar, S. S.; Tomasi, J.; Cossi, M.; Millam, J. M.; Klene, M.; Adamo, C.; Cammi, R.; Ochterski, J. W.; Martin, R. L.; Morokuma, K.; Farkas, O.; Foresman, J. B.; Fox, D. J. *Gaussian 1*. Revision B.01; Gaussian Inc.: Wallingford CT, 2016.

DOI: 10.1021/acs.jctc.9b00689
J. Chem. Theory Comput. XXXX, XXX, XXX−XXX

(36) Breneman, C. M.; Wiberg, K. B. Determining atom-centered monopoles from molecular electrostatic potentials. The need for high sampling density in formamide conformational analysis. *J. Comput. Chem.* **1990**, *11*, 361.
(37) Plimpton, S.; Comp, J. Fast Parallel Algorithms for Short-Range Molecular Dynamics. *Phys.* **1995**, *117*, 1.
(38) Padua, A. A. H. *fftool*. github.com/agiliopadua/fftool, 2013.
(39) Martínez, L.; Andrade, R.; Birgin, E. G.; Martínez, J. M. PACKMOL: A package for building initial configurations for molecular dynamics simulations. *J. Comp. Chem.* **2009**, *30*, 2157.
(40) Padua, A. A. H. *fftool*. github.com/agiliopadua/fftool, 2019.
(41) Canongia Lopes, J. N.; Pádua, A. A. H. Molecular Force Field for Ionic Liquids Composed of Triflate or Bistriflylimide Anions. *J. Phys. Chem. B* **2004**, *108*, 16893.
(42) Gouveia, A. S. L.; Bernardes, C. E. S.; Tomé, L. C.; Lozinskaya, E. I.; Vygodskii, Y. S.; Shaplov, A. S.; Lopes, J. N. C.; Marrucho, I. M. Ionic liquids with anions based on fluorosulfonyl derivatives: from asymmetrical substitutions to a consistent force field model. *Phys. Chem. Chem. Phys.* **2017**, *19*, 29617.
(43) Thole, B. T. Molecular polarizabilities calculated with a modified dipole interaction. *Chem. Phys.* **1981**, *59*, 341.
(44) Noskov, S. Y.; Lamoureux, G.; Roux, B. Molecular Dynamics Study of Hydration in Ethanol−Water Mixtures Using a Polarizable Force Field†. *J. Phys. Chem. B* **2005**, *109*, 6705.
(45) Maginn, E. J.; Messerly, R. A.; Carlson, D. J.; Roe, D. R.; Elliott, J. R. Best Practices for Computing Transport Properties 1. Self-Diffusivity and Viscosity from Equilibrium Molecular Dynamics [Article v1.0]. *Living J. Comp. Mol. Sci.* **2019**, *1*. DOI: 10.33011/livecoms.1.1.6324.
(46) Hirschfelder, J. O.; Curtiss, C. F.; Bird, R. B. *Molecular Theory of Gases and Liquids*; Wiley, 1954, p 1280.
(47) Brereton, R. G. *Applied Chemometrics for Scientists*; Wiley, 2007, p 396.
(48) Noda, A.; Hayamizu, K.; Watanabe, M. Pulsed-Gradient Spin−Echo1H and19F NMR Ionic Diffusion Coefficient, Viscosity, and Ionic Conductivity of Non-Chloroaluminate Room-Temperature Ionic Liquids. *J. Phys. Chem. B* **2001**, *105*, 4603.
(49) Nieto de Castro, C. A.; Langa, E.; Morais, A. L.; Lopes, M. L. M.; Lourenço, M. J. V.; Santos, F. J. V.; Santos, M. S. C. S.; Lopes, J. N. C.; Veiga, H. I. M.; Macatrão, M.; Esperança, J. M. S. S.; Marques, C. S.; Rebelo, L. P. N.; Afonso, C. A. M. Studies on the density, heat capacity, surface tension and infinite dilution diffusion with the ionic liquids [C4mim][NTf2], [C4mim][dca], [C2mim][EtOSO3] and [Aliquat]-[dca]. *Fluid Phase Equil.* **2010**, *294*, 157.
(50) França, J. M. P.; Reis, F.; Vieira, S. I. C.; Lourenço, M. J. V.; Santos, F. J. V.; Nieto de Castro, C. A.; Pádua, A. A. H. Thermophysical properties of ionic liquid dicyanamide (DCA) nanosystems. *J. Chem. Thermodyn.* **2014**, *79*, 248.
(51) Neves, C. M. S. S.; Kurnia, K. A.; Coutinho, J. A. P.; Marrucho, I. M.; Lopes, J. C.; Freire, M. G.; Rebelo, L. P. N. Systematic Study of the Thermophysical Properties of Imidazolium-Based Ionic Liquids with Cyano-Functionalized Anions. *J. Phys. Chem. B* **2013**, *117*, 10271.
(52) Sánchez, L. G.; Espel, J. R.; Onink, F.; Meindersma, G. W.; Haan, A. d. Density, Viscosity, and Surface Tension of Synthesis Grade Imidazolium, Pyridinium, and Pyrrolidinium Based Room Temperature Ionic Liquids. *J. Chem. Eng. Data* **2009**, *54*, 2803.
(53) Tokuda, H.; Hayamizu, K.; Ishii, K.; Susan, M. A. B. H.; Watanabe, M. Physicochemical Properties and Structures of Room Temperature Ionic Liquids. 1. Variation of Anionic Species. *J. Phys. Chem. B* **2004**, *108*, 16593.
(54) Tokuda, H.; Hayamizu, K.; Ishii, K.; Susan, M. A. B. H.; Watanabe, M. Physicochemical Properties and Structures of Room Temperature Ionic Liquids. 2. Variation of Alkyl Chain Length in Imidazolium Cation. *J. Phys. Chem. B* **2005**, *109*, 6103.
(55) Tokuda, H.; Ishii, K.; Susan, M. A. B. H.; Tsuzuki, S.; Hayamizu, K.; Watanabe, M. Physicochemical Properties and Structures of Room-Temperature Ionic Liquids. 3. Variation of Cationic Structures. *J. Phys. Chem. B* **2006**, *110*, 2833.
(56) Harris, K. R.; Kanakubo, M. Revised and Extended Values for Self-Diffusion Coefficients of 1-Alkyl-3-methylimidazolium Tetrafluoroborates and Hexafluorophosphates: Relations between the Transport Properties. *J. Phys. Chem. B* **2016**, *120*, 12937.
(57) Chirico, R. D.; Diky, V.; Magee, J. W.; Frenkel, M.; Marsh, K. N. Thermodynamic and thermophysical properties of the reference ionic liquid: 1-Hexyl-3-methylimidazolium bis[(trifluoromethyl)sulfonyl]-amide (including mixtures). Part 2. Critical evaluation and recommended property values (IUPAC Technical Report). *Pure Appl. Chem.* **2009**, *81*, 791.
(58) Freire, M. G.; Teles, A. R. R.; Rocha, M. A. A.; Schröder, B.; Neves, C. M. S. S.; Carvalho, P. J.; Evtuguin, D. V.; Santos, L. M. N. B. F.; Coutinho, J. A. P. Thermophysical Characterization of Ionic Liquids Able To Dissolve Biomass. *J. Chem. Eng. Data* **2011**, *56*, 4813.
(59) Zec, N.; Bešter-Rogač, M.; Vraneš, M.; Gadžurić, S. Physicochemical properties of (1-butyl-1-methylpyrrolydinium dicyanamide + γ-butyrolactone) binary mixtures. *J. Chem. Thermodyn.* **2015**, *91*, 327.
(60) Simons, T. J.; Bayley, P. M.; Zhang, Z.; Howlett, P. C.; MacFarlane, D. R.; Madsen, L. A.; Forsyth, M. Influence of Zn2+ and Water on the Transport Properties of a Pyrrolidinium Dicyanamide Ionic Liquid. *J. Phys. Chem. B* **2014**, *118*, 4895.
(61) Radhi, A.; Le, K. A.; Ries, M. E.; Budtova, T. Macroscopic and Microscopic Study of 1-Ethyl-3-methyl-imidazolium Acetate-DMSO Mixtures. *J. Phys. Chem. B* **2015**, *119*, 1633.
(62) Oliveira, F. S.; Rebelo, L. P. N.; Marrucho, I. M. Influence of Different Inorganic Salts on the Ionicity and Thermophysical Properties of 1-Ethyl-3-methylimidazolium Acetate Ionic Liquid. *J. Chem. Eng. Data* **2015**, *60*, 781.
(63) Pereiro, A. B.; Araújo, J. M. M.; Oliveira, F. S.; Bernardes, C. E. S.; Esperança, J. M. S. S.; Canongia Lopes, J. N.; Marrucho, I. M.; Rebelo, L. P. N. Inorganic salts in purely ionic liquid media: the development of high ionicity ionic liquids (HIILs). *Chem. Commun.* **2012**, *48*, 3656.
(64) Araújo, J. M. M.; Pereiro, A. B.; Alves, F.; Marrucho, I. M.; Rebelo, L. P. N. Nucleic acid bases in 1-alkyl-3-methylimidazolium acetate ionic liquids: A thermophysical and ionic conductivity analysis. *J. Chem. Thermodyn.* **2013**, *57*, 1.
(65) McDaniel, J. G.; Choi, E.; Son, C. Y.; Schmidt, J. R.; Yethiraj, A. Ab Initio Force Fields for Imidazolium-Based Ionic Liquids. *J. Phys. Chem. B* **2016**, *120*, 7024.
(66) McDaniel, J. G.; Son, C. Y.; Yethiraj, A. Ab Initio Force Fields for Organic Anions: Properties of [BMIM][TFSI], [BMIM][FSI], and [BMIM][OTf] Ionic Liquids. *J. Phys. Chem. B* **2018**, *122*, 4101.

DOI: 10.1021/acs.jctc.9b00689
J. Chem. Theory Comput. XXXX, XXX, XXX−XXX